International Journal of GEOMATE, Feb., 2021, Vol.20, Issue 78, pp. 165-170
ISSN: 2186-2982 (P), 2186-2990 (O), Japan, DOI: https://doi.org/10.21660/2021.78.GX201
Geotechnique, Construction Materials and Environment

STRESS ANALYSIS OF RIVER EMBANKMENT CONSIDERING EXTERNAL WATER LEVEL FLUCTUATION

Tsubasa Ichijo [1] and *Shin-ichi Kanazawa [2]

[1] Social Environmental Systems Engineering Course, National Institute of Technology, Fukushima College, Advanced Course Program, Japan;
[2]Civil and Environmental Engineering, National Institute of Technology, Fukushima College, Japan,

*Corresponding Author, Received: 15 June 2020, Revised: 30 Nov. 2020, Accepted: 17 Jan. 2021

ABSTRACT: In recent years, local downpours frequently occur in various parts of Japan, and embankments are destroyed by these downpours. Many embankments are historical products of flood control that have been reinforced as they age by raising their height. However, the structure of the river embankment was developed based on information from disasters that actually occurred, and analysis of the destruction of the structure was not considered in design. Furthermore, until now, mechanisms of levee collapse have been discussed, but they have not been fully elucidated. Therefore, in this study, embankment analysis considering difference of layer thickness was performed by using the unsaturated soil / water / air coupled element finite method analysis program (DACSAR-MP). Stress behavior in the embankment during the rise of the river water level due to rainfall was analytically expressed, and the effect of the stress was considered to analytically investigate the collapse mechanism of the river embankment. From this work, it was analytically confirmed that embankment failure mode differed depending on differences in the speed of water level rise.

Keywords: River embankment, Unsaturated soil, Penetration, Collapse

1. INTRODUCTION

Due to global climate change, there have been frequent reports of local torrential rains in various parts of Japan in recent years, with associated river dike collapse. Among these, the breach of the embankment of the Chikuma River caused by Typhoon No.19 in October 2019 stands out. An embankment is an extremely important disaster prevention structure that protects the lives of riverside residents from floods, and it is necessary to ensure the safety of these structures.

Regarding water infiltration resistance, erosion resistance and seismic resistance ratings required for river levees, the existing rules for satisfying the earth levee principle and cross-sectional shape have been revised, and the magnitude of the external force applied to the levees before the earth structure is constructed has been stipulated. As a general rule, the design of levees for each river should be optimized considering topography, weather, and river shape. However, the mechanism of destabilization and deformation of levees due to floods or earthquakes has not yet been fully elucidated [1], and the current guidelines do not necessarily represent well-established technical knowledge.

On the other hand, the difficulty of elucidating the mechanisms of river levee infiltration and stability problems is because these problems deal with unsaturated soil, intermediate soil, compacted soil and unsteady phenomena. Overflow, erosion, seepage, and earthquakes are the causes of riverbank breakage due to changes in the outside water level. Of these, all except for earthquakes are caused by rainfall, and the risk of riverbank breakage is increasing due to the recent local heavy rainfall. Currently, as an evaluation method for embankment structures, arc slip analysis is performed using the infiltration analysis results, such as rainfall, in the embankment design method Nonetheless, deformation analysis is not performed, and infiltration analysis and stability analysis are performed individually. However, the infiltration problem and the deformation problem are coupled, and it is hard to say that the current embankment evaluation method is sufficient.

It is thought that local torrential rain will increase in the future, and it can be said that the risk of bank breakage will increases alongside this. Since the damage caused by river embankment is enormous, it is urgent to take measures against embankment failure, and for that purpose, it is important to elucidate the destruction mechanism of the river embankment.

In previous studies, Kodaka, Lee, Kubo, Ishihara, Nakayama, Li, and Fujita [2] have investigated the stress state and collapse mechanism inside the embankment using their respective methods, but all of them are in service. On the other hand, there is no discussion about continuous state changes and rainfall intensity.

In this study, using the unsaturated soil / water / air coupled element finite method analysis program

(DACSAR-MP) [3], we focused on embankment reinforcement and conducted the embankment analysis considering differences in layer thickness. The purpose of this study is to analytically elucidate river levee collapse mechanisms by analytically expressing the stress behavior in the levee body during river water level rise due to and considering the effect of rainfall. In addition, by changing the water level rise speed, we can see the difference in the fracture form due to the difference in speed.

2. RESEARCH METHOD

2.1 Soil/Water/Air Coupled Finite Analysis Code

The finite element analysis code (DACSAR-MP) [3] used in this study formulates the unsaturated soil constitutive model proposed by Ohno, Kawai, and Tachibana [4]. This model is framed as the soil/water/air coupled problem using the three-phase mixture theory. Equation (1) shows the effective stress. Equation (2) shows the base stress tensor and suction stress. Equation (3) shows suction.

$$\boldsymbol{\sigma}' = \boldsymbol{\sigma}^{\mathbf{net}} + p_s \mathbf{1} \tag{1}$$

$$\boldsymbol{\sigma}^{\mathbf{net}} = \boldsymbol{\sigma} - p_a \mathbf{1}, \;\; p_s = S_e s \tag{2}$$

$$s = p_a - p_w, S_e = \frac{S_r - S_{rc}}{1 - S_{rc}} \tag{3}$$

Here, $\boldsymbol{\sigma}'$ is the effective stress tensor; $\boldsymbol{\sigma}^{\mathbf{net}}$ is the base stress tensor; $\mathbf{1}$ is the second order unit tensor; $\boldsymbol{\sigma}$ is the total stress tensor; s is the suction; p_s is the suction stress; p_a is the pore air pressure; p_w is the pore water pressure; S_r is the degree of saturation; S_e is the effective degree of saturation; and S_{rc} is the degree of saturation at s→∞. Equations (4), (5), (6) and (7) provide the yield function.

$$f\left(\boldsymbol{\sigma}', \zeta, \varepsilon_v^p\right) = MD \ln \frac{p'}{\zeta p_{sat}'} + \frac{MD}{n_E}\left(\frac{q}{Mp'}\right)^{n_E} - \varepsilon_v^p = 0 \tag{4}$$

$$\zeta = \exp\left[\left(1 - S_e\right)^{n_s} \ln a\right], MD = \frac{\lambda - \kappa}{1 + e_0} \tag{5}$$

$$p' = \frac{1}{3}\boldsymbol{\sigma}' : \mathbf{1}, q = \sqrt{\frac{3}{2}\mathbf{s} : \mathbf{s}} \tag{6}$$

$$\mathbf{s} = \boldsymbol{\sigma}' - p'\mathbf{1} = \mathbf{A} : \boldsymbol{\sigma}', \mathbf{A} = \mathbf{I} - \frac{1}{3}\mathbf{1} \otimes \mathbf{1} \tag{7}$$

Here, n_E is the shape parameter; ε_v^p is the plastic volume strain; M is the q/p' in the limit state; D is the dilatancy coefficient; p_{sat}' is the yield stress at saturation; a and n_s are the parameters representing the increase in yield stress due to unsaturation; λ is the compression index; and κ is the expansion index. Equation (8) shows pore water velocity. Equation (9) shows air velocity. Pore water and air flow follow Darcy's law.

$$\tilde{v}_{\mathrm{w}} = -\mathbf{k}_{\mathbf{w}} \cdot \mathrm{grad} h \tag{8}$$

$$\tilde{v}_{\mathrm{a}} = -\mathbf{k}_{\mathbf{a}} \cdot \mathrm{grad} h_a, h_a = \frac{p_a}{\gamma_w} \tag{9}$$

Here, $\tilde{v}_{\mathrm{w}}$ is the pore water velocity; $\tilde{v}_{\mathrm{a}}$ is the air velocity; $\mathbf{k}_{\mathbf{w}}$ is the hydraulic conductivity; $\mathbf{k}_{\mathbf{a}}$ is the coefficient of air permeability; h is the total head; γ_w is the unit weight of water; and h_a is the pneumatic head. Equations (10)-(11) show hydraulic conductivity and the coefficient of air permeability by way of Mualem's [5] formula and the Van Genuchten [6] formula.

$$\mathbf{k}_{\mathbf{w}} = k_{rw}\mathbf{k}_{\mathbf{wsat}} = S_e^{1/2}\left[1 - \left(1 - S_e^{1/m}\right)^m\right]^2 \mathbf{k}_{\mathbf{wsat}} \tag{10}$$

$$\mathbf{k}_{\mathbf{a}} = k_{ra}\mathbf{k}_{\mathbf{ares}} = \left(1 - S_e\right)^{1/2}\left(1 - S_e^{1/m}\right)^{2m} \mathbf{k}_{\mathbf{ares}} \tag{11}$$

Here, k_{rw} is the ratio of hydraulic conductivity; k_{ra} is the ratio of coefficient of air permeability; m is the Mualem constant; $\mathbf{k}_{\mathbf{wsat}}$ is the hydraulic conductivity at saturation; $\mathbf{k}_{\mathbf{ares}}$ is the coefficient of air permeability in dry conditions. Equations (12)-(13) show the continuous formula of pore water and air using three-phase mixture theory.

$$n\dot{S}_r - S_r\dot{\varepsilon}_v + \mathrm{div}\tilde{v}_w = 0 \tag{12}$$

$$\left(1 - S_r\right)\dot{\varepsilon}_v + n\dot{S}_r - n\left(1 - S_r\right)\frac{\dot{p}_a}{p_a + p_0} - \mathrm{div}\tilde{v}_a = 0 \tag{13}$$

Here, n is porosity; $\dot{\varepsilon}_v$ is volumetric strain; and p_0 is atmospheric pressure. The elasto-plastic constitutive model obtained from Equation (4) and the equilibrium equation [Equations (12) - (13)] are formulated as the soil/water/air coupled problem.

2.2 Moisture Characteristic Curve Used in the Analysis

For a soil-water characteristic curve model, a model capable of hysteresis expression, as proposed by Kawai, Wang and Iizuka [7], is used. In addition, to determine the logistic curve in the case of DRY and WET, derived from arbitrary suction and the

degree of saturation, the logistic curve equation of Sugii and Uno [8] was used. This makes it possible to grasp the moisture conditions of sloped ground where complex water balance occurs.

3. INTERIOR CHANGES IN THE DIKE WITH EMBANKMENT COMPLETION

3.1 Analysis Conditions

Figure 1 shows the analytical model. The foundation ground was 3m long and 45m long, and the dam body was 5m long, 5m at the top, and 25m at the bottom, with a slope of 1: 2 [9]. The mesh of the model is 1m each for the foundation ground, 10 cm for the levee body, and it was divided into 25 parts horizontally. The right side of the analytical model was assumed to be the river side, and the drainage layer was 0.6m in length and 6m in width from the left end of the embankment.

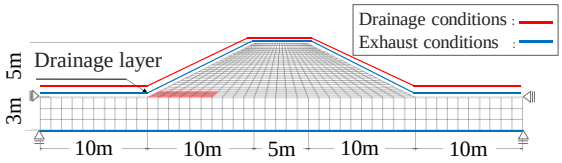

Fig. 1 Finite element mesh diagram

The material used in the analysis was silt mixed with sand for the foundation ground and sand mixed with silt for the dam body. Table 1 shows the material constants, and Figure 3 shows the moisture characteristic curve. Table 1.1 is the material constant used for the foundation ground, and Table 1.2 is the material constant used for the dam body. Figure 2.1 shows the moisture characteristic curve used for the foundation ground, and Figure 2.2 shows the moisture characteristic curve used for the dam body. The material constants shown in Table 1 are λ: swelling index, k: compression index, M: critical stress ratio, m: shape parameter of unsaturated hydraulic conductivity, n: magnification parameter of consolidation yield stress in unsaturated state, nE: Fitting parameter of EC model, e_0: Initial void ratio, ν: Poisson's ratio, k_x: Horizontal hydraulic conductivity, K_Y: vertical hydraulic conductivity, S_{r0}: critical saturation, and G_s: soil particle specific gravity. The initial saturation of the material used for embankment was set to 60%, and the initial suction was determined from Figure2.2. The drainage layer has a permeability coefficient and an air permeability coefficient set to 500 times that of the embankment. The material constants other than the permeability coefficient and the permeability coefficient of the drainage layer are the same as those of the bank body. The displacement boundary was fixed vertically at the bottom of the foundation ground and horizontally at the top of the foundation ground.

For the hydraulic boundary, the lower and upper ends of the foundation ground and the upper part of the dam body were drained. As for the air boundary, the upper end of the foundation ground and the upper end of the dam were exhausted.

3.2 Analysis Method

Table 1.1 Foundation ground material parameters

λ	k	M	m	n	nE
0.18	0.037	1.33	0.8	1	1.3
e_0	ν	kx(m/day)	ky(m/day)	Sr_0	Gs
1.2	0.33	0.1	0.1	0.15	2.7

Table 1.2 Levee material parameters

λ	k	M	m	n	nE
0.18	0.013	1.33	0.8	1	1.3
e_0	ν	kx(m/day)	ky(m/day)	Sr_0	Gs
1	0.33	8.7	8.7	0.15	2.7

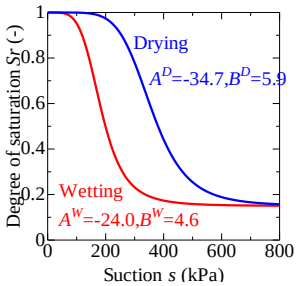

Fig.2.1 Soil-water characteristic curve (Foundation ground)

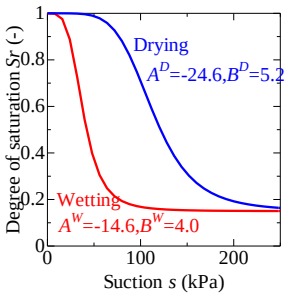

Fig. 2.2 Soil-water characteristic curve (Levee)

In the embankment analysis, layers were spread one-by-one. An evenly distributed load was applied, and compaction was repeated until the height of the embankment reached 5m. Layers of 0.3m and 0.6m were prepared. The rolling strength was 300kPa. In the analysis, elements were generated to create a heap, and loading and unloading was repeated with an evenly distributed load to simulate compaction. This schematic diagram is shown in Figure 3.

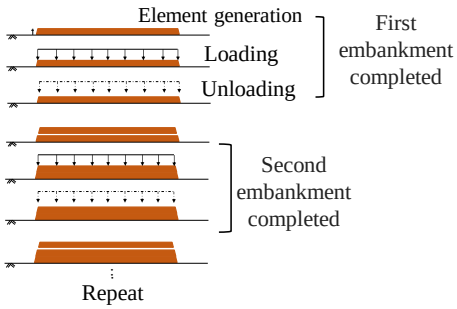

Fig.3 Embankment analysis schematic

3.3 Analysis Result

Figure 4 shows a visualization of each stress at the completion of the embankment (layer thickness: left 0.3 m, right 0.6m). From the top, the mean effective stress *p'*, void ratio *e*, deviatoric stress *q*, shear strain ε_s, suction *s*, and degree of saturation S_r are shown. First, the mean effective stress *p'* exhibits a higher value in the foundation ground than in the embankment due to the effect of compaction during embankment construction. In addition, the gap ratio e is higher toward the upper part of the levee body, and the layer thickness of 0.6m is particularly remarkable in this respect. Next, the shear strain ε_s shows a higher value near the boundary between the foundation and the levee than in the levee.

Therefore, it is possible that there was already weakening when the embankment was completed, although not enough to cause failure. In addition, as the position where the drainage layer is located contains more water than the surrounding area, the void ratio *e* is low. Comparing layer thickness, the value of 0.6m shows smaller mean effective principal stress, and the gap ratio e is larger in the upper part of the dam body. At 0.6m, layer boundaries occur at the mean effective stress *p'*, the void ratio *e*, and the deviatoric stress *q*. Therefore, it is considered that the levee body compacted with a layer thickness of 0.6m has a discontinuity at the layer boundary, in contrast to the lack of this discontinuity with 0.3m layer thickness, resulting from insufficient compaction.

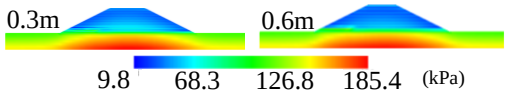

(i) Mean effective stress *p'*

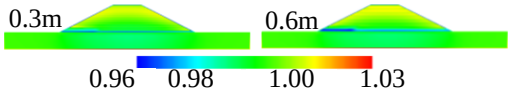

(ii) Void ratio *e*

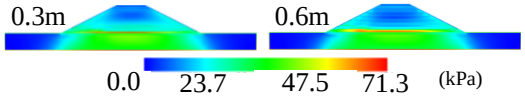

(iii) Deviatoric stress *q*

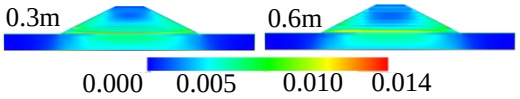

(iv) Shear Strain ε_s

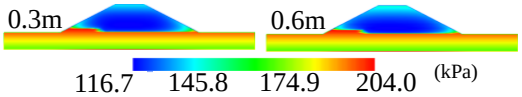

(v) Suction *s*

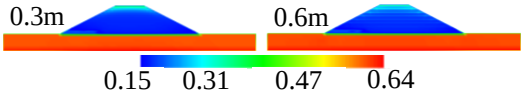

(vi) Degree of saturation S_r

Fig. 4 Summarizes analysis results

4. CHANGES IN THE LEVEL DUE TO RISINGWATER LEVELS

Water level fluctuation analysis was carried out using the analytical model used for embankment analysis. The right side of the embankment was used to raise the water level. This is expressed by applying water pressure to the levee body and the foundation ground after raising the head of water on the right slope of the embankment where water infiltrates, along with the foundation ground. The water head and water pressure applications were repeated until the crown reached 3m. In addition, the rate of water level rise was set to 1.4cm /min and 14cm/min [10]. (Rise rate: (A)1.4cm /min, (B)14cm/min)

Next, we paid attention to the difference in the speed of water level rise. Figure 5 shows the analysis results for each stress. Each figure shows the average effective principal stress *p'*, axial differential stress *q*, shear strain ε_s, void ratio e, suction s, and degree of saturation S_r from the top. From the left of the figure, the water level of each stress is extracted at 1.5m and 3m.

First, from results of the mean effective stress *p'*, strength is considered to decrease as the water level rises, and the value inside the levee decreases from the infiltration surface. In addition, the void ratio *e* also decreases inside the levee from the infiltration surface as the water level rises, and volume compression is considered to occur. Second, from the degree of saturation S_r, it can be seen that values

for the foundation ground and the lower part of the levee become lower as the water level rises. At a slower velocity of (A)1.4cm/min this value is higher than at a faster velocity of (B)14cm/min. Finally, the shear strain ε_s indicates that the value at the tail end of the embankment is higher, suggesting that the tail end becomes a weak part of the embankment as the water level rises. For each stress, the change in velocity in (A) was more remarkable than that in (B). This is probably because at the slower the rising speed, the infiltration time of the river water was longer. In particular, the degree of saturation S_r was significantly different with different rising speeds, and a large difference in the formation of the infiltration surface was confirmed. The velocity (A) formed a smooth infiltration surface, and the velocity (B) formed a vertical infiltration surface. It is considered that (A) first infiltrated from the foundation ground and then infiltrated upward from the ground to the bank body.

At this time, the levee body can be considered as subject to buoyancy due to leftward infiltration

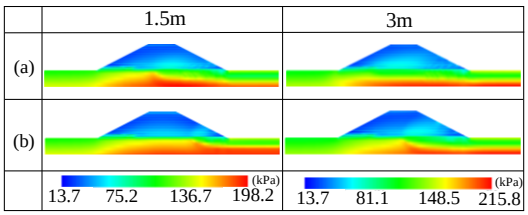

(i) Mean effective stress p'

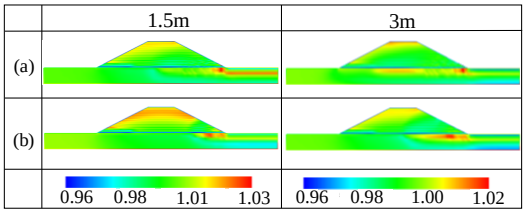

(ii) Void ratio e

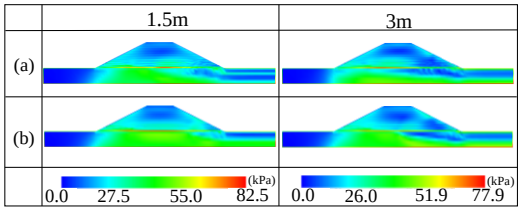

(iii) Deviatoric stress q

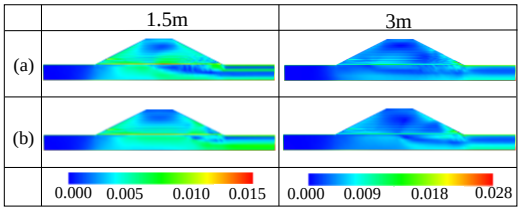

(iv) Shear Strain ε_s

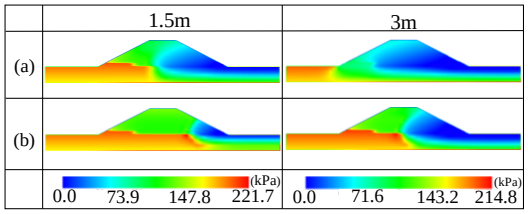

(v) Suction s

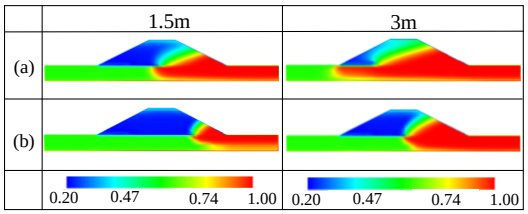

(vi) Degree of saturation S_r

Fig. 5 Summarizes analysis results

from the levee exterior and upward infiltra tion from the foundation ground, suggesting the possibility of piping. In contrast to (A), (B) is considered to have caused infiltration only from the lower left side of the embankment to form a vertical infiltration surface, suggesting that water overflow may occur.

Furthermore, in order to study the detailed behavior of saturation S_r in the levee, changes in the water level rise of the elements in the levee are visualized graphically. The position of each element is shown in Figure 6, and the behavior in the ascending process is shown in Figure 7 (Figure 7.1: 1.4cm/min, Figure 7.2: 14cm/min). The graph shows the time (unit:day) horizontally and the saturation S_r vertically. From Figure 7.1, it can be confirmed that not only the elements 126, 160, 885 and 1385, but also the element 113 and the elements 101 and 187, are changing from the unsaturated state to the saturated state. From this, water is considered to have penetrated to the inner side of the bank, forming water channels, and this result also suggests that piping may occur. Because all the elements located on the foundation ground are saturated and element 101 is saturated earlier than element 187 on the ground side of the embankment, it can be confirmed that water permeates from the foundation ground earlier than from the embankment exterior. Figure 7.2, shows that the time required for saturation of each element remains almost unchanged, and that the levee body is saturated at a stretch in a short time compared to the speed of 1.4cm/min. From this, it is possible to confirm the vertical infiltration in the levee body, and it is unlikely that water channels form.

Therefore, it is considered that the slower the rising speed is, the higher the possibility of water channel formation.

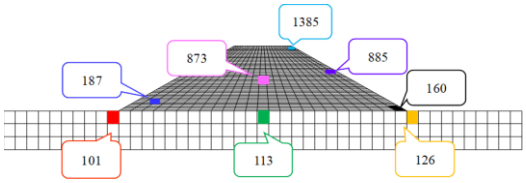

Fig.6 Position of each element

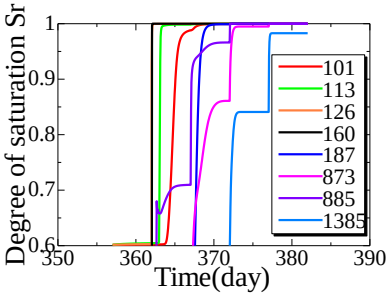

Fig.7.1 Transition of saturation of each element

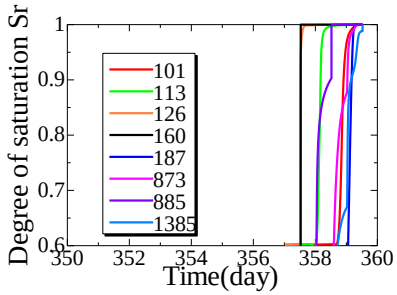

Fig.7.2 Transition of saturation of each element

5. CONCLUSION

Based on the results obtained from the embankment analysis and the water level rise analysis, the following conclusions are developed.

(1) When the layer thickness is large, the average effective principal stress *p'* and the void ratio *e* are small at the completion of the embankment, resulting in a discontinuity at the layer boundary. When the water level rises, the osmotic pressure of the outer water level is dominant, and therefore, the dominance of collapse due to the change in layer thickness was not observed. Therefore, it was confirmed that the difference in height of padding did not significantly affect the infiltration, and destruction was caused mainly by infiltration due to the rise of the water level.

(2) As the water level rises, the strength inside the levee decreases, the volume is compressed, and the inside of the levee is saturated, thus collapse is considered to occur within the levee. In addition, collapse progresses into the levee body as the water level rises.

(3) When the rate of water level rise is slow there is a high possibility of collapse due to the long infiltration time of river water. If the ascending speed is high, it is likely that the river will overtop the levee before collapse occurs.

(4) A gentle infiltration surface formed when the speed of water level rise was slow, and a vertical infiltration surface was formed when the water velocity was high. In particular, when the speed is slow, the dam body may be subjected to upward penetration from the foundation ground in addition to leftward penetration from the outside of the embankment. This results in buoyancy and the formation of water channels in the foundation ground to cause Penetration destruction.

6. REFERENCES

[1] Japan Institute of Country-ology and Engineering：River embankment guide (Revised edition),2012, p.1.

[2] Kodaka T., Lee K., Kubo Y., Ishihara M., Nakayama Y., Li Z., Fujita K: Shear Strength Test Method for River Embankment Penetration, Proceedings of the 7th River Embankment Symposium, 2019, p.35.

[3] Kanazawa S., Toyoshima K., Kawai K., Tachibana S. and Iizuka, A.: Analysis of mechanical behavior of compacted soil with F.E. method, journal of JSCE, No.68 (2), 2012, pp.291-298.

[4] Ohno S., Kawai K. and Tachibana S.: Elastoplastic constitutive model for unsaturated soil applied effective degree of saturation as a parameter expressing stiffness, Journal of JSCE, Vol.63/No.4,2007, pp.1132-1141.

[5] Mualem Y.: A new model for predicting the hydraulic conductivity of unsaturated porous media, Water Re-sources Research, Vol.12, No.3, 1976, pp.514-522.

[6] Van Genuchten: A closed-form equation for predicting hydraulic of unsaturated soils, Soil Science Society American Journal, Vol.44, 1980, pp.892-898.

[7] Kawai K., Wang W. and Iizuka, A.: The expression of hysteresis appearing on water characteristic curves and the change of stresses in unsaturated soils, Journal of applied mechanics, Vol.5, 2002, pp.777-784.

[8] Sugii T. and Uno T: Modeling the New Moisture Characteristic Curve, Journal of JSCE, 1995, pp.130-131.

[9] Japan Road Association,:Roadway Workers - Fill Construction Guidelines, 2010, p.163.

[10] Ministry of Land, Infrastructure, Tranceport and Tourism Hokuriku Regional Development Bureau:Chikuma River Embankment Survey Committee materials, 2019, p.8.